Research

Photostability, cytotoxicity, and photothermal impact of AgNPs, CoAgNC, and IOAgNC on HEp-2 laryngeal carcinoma cells

Marwa A. Ramadan[1] · **Tarek A. El-Tayeb**[1]

Received: 1 June 2023 / Accepted: 15 August 2023
Published online: 29 August 2023

Abstract
Magnetic nanoparticles have shown promise in various medical applications, including cancer treatment and diagnostics. The objective of this study is to attain mastery over the synthesis of silver nanoparticles (AgNPs), Cobalt silver nanocomposite (CoAgNC) and magnetite silver nanocomposite (IOAgNC), while also examining their photostability, cytotoxicity, and photothermal impact on Human Laryngeal Carcinoma Cell line (HEp-2). The preparation and characterization of AgNPs, CoAgNC, and IOAgNC were described, including the assessment of their photostability and cytotoxicity on HEp-2 cell line. The photostability of these nanomaterials was determined by subjecting them to different light sources, while their morphology and magnetic properties were characterized using a spectrophotometer, Transmission Electron Microscopy (TEM), and Vibrating Sample Magnetometer (VSM). The results of the characterization of AgNPs, CoAgNC, and IOAgNC showed that the prepared nanomaterials have distinct optical and morphological properties. The synthesized nanomaterials were stable in aqueous solutions and exhibited magnetic properties. The cytotoxicity tests on HEp-2 cells showed that the nanomaterials were not toxic in the dark, but their toxicity increased under light exposure, with IOAgNC showing the most significant toxicity. CoAgNC was found to be photostable under UV light and Light Emitting Diode (LED) irradiation due to the little lattice mismatch between cobalt and silver. Nanocomposite systems of high magnetic moment, such as IOAgNC and CoAgNC, have potential for tumor treatment through magnetic fluid hyperthermia. The photostability, chemical stability, and biocompatibility of AgNPs, CoAgNC, and IOAgNC were investigated and found to be non-toxic even at high concentrations. These nanomaterials have multiple optical and magnetic functionalities and are promising candidates for biomedical applications.

Article Highlights

- AgNPs, CoAgNC, and IOAgNC exhibit distinct optical and morphological properties, showing promise for diverse applications.
- While these nanomaterials are non-toxic in darkness, they exhibit increased toxicity when exposed to light, with IOAgNC displaying the highest toxicity.
- IOAgNC and CoAgNC have potential for tumor treatment using magnetic fluid hyperthermia, while AgNPs, CoAgNC, and IOAgNC are shown to be biocompatible and stable.

✉ Marwa A. Ramadan, marwali_mus@cu.edu.eg | [1]Department of Laser Application in Metrology Photochemistry and Agriculture, National Institute for Laser Enhanced Science (NILES), Cairo University (CU), Giza, Egypt.

Keywords Silver nanoparticles (AgNPs) · Cobalt silver nanocomposite (CoAgNC) · Magnetite silver nanocomposite (IOAgNC) · Photostability · Cytotoxicity · PTT · HEp-2 cell line

1 Introduction

In recent times, there has been a growing interest in developing alternative high-momentum metal nanomaterials, such as Co, Fe, and related alloys, for specific biomedical applications like bioseparation and targeted delivery [1–5]. Among the assorted metal oxide nanoparticles, magnetic nanoparticles have been widely studied for different chemical and biological applications. The low biocompatibility and susceptibility to oxidation in oxygen-rich settings of magnetic nanoparticles limits their utility in biological applications. Consequently, significant efforts have been made to create a biocompatible interface by producing magnetic optical nanocomposites. These nanocomposites have gained considerable attention as they offer two or more nanoscale functionalities that can facilitate easy and crucial biomedical/diagnostic applications with enhanced detection sensitivity [6–9]. Magnetic nanoparticles are well-known for their potential applications in biomedical fields, such as cell labeling and isolation [10], magnetic resonance imaging (MRI) [11], target drug delivery, magnetic ferrofluids hyperthermia (MFH) [12–14], and controlled drug targeting delivery [15, 16]. The synthesis of magnetic/metal nanoparticles with controllable size is not widely documented. One report states that the synthesis of water-soluble magnetite/gold nanoparticles improves biocompatibility and chemical stability by safeguarding the magnetic nanoparticles from further oxidation [17]. The application of magnetic nanoparticles in photothermal therapy platforms has been significantly researched, as light absorption-induced heat can cause cellular responses such as apoptosis by increasing reactive oxygen species (ROS) levels and can be locally destroyed by hyperthermia during photothermolysis, thus targeting sites without causing substantial side effects in neighboring normal tissue [18].

Cobalt and magnetite nanoparticles have attracted interest, especially in medical applications such as diagnostics [19], hyperthermia cancer treatment [20]. This is due to their properties such as biocompatibility [17], biodegradability [21, 22], magnetic behavior, [17] and the possibility of easy functionalization [23]. In noble metals, coherent collective vibrations of electrons in the conduction band induce large surface electric fields, which enhance the radiation properties of metal nanoparticles when they interact with resonant electromagnetic radiation [24, 25]. These unique properties enable scientists, engineers, and physicians to produce major advances in the life sciences and health care as in molecular biology, bioengineering, medical diagnostics, and therapeutics [26, 27]. A particularly interesting class is nanocomposites. These nanocomposites are highly functional materials consisting of a thin coating (1–20 nm) of one material deposited on particle of another different material using specific techniques [28–30]. It is now possible to synthesize these nanocomposites with desired dimensions [31]. Nanocomposites can be synthesized using a method called controlled precipitation [32]. The choice of a suitable pair for the nanocomposites requires the understanding of individual properties of each nanoparticle material. Because of potential applications associated with them, nanocomposites have gained considerable attention in recent years. They have been synthesized for a variety of applications like fluorescent diagnostic labels in imaging cancer cells and other therapeutic applications [5, 33], enhancement of luminescence properties [34], preparation of bio conjugates [35] and increasing chemical and photostability of colloids [36].

In this study, we present the aqueous synthesis of IOAgNC and CoAgNC. Due to their multiple optical and magnetic functionalities, these nanosystems hold significant potential for various biological applications, particularly in medical sensors and biomedicine. This is attributed to the strong magnetic moment signal and well-established silver chemistry, which allows for a broad range of surface modification strategies, thus enabling biocompatibility and stability. The primary objective of this research is to achieve precise control over the synthesis of AgNPs, CoAgNC, and IOAgNC, while also investigating their photostability, cytotoxicity, and photothermal effects on the HEp-2 laryngeal carcinoma cell line.

2 Material and methods

2.1 1-Preparation of spherical AgNPs

To prepare spherical AgNPs, a mixture of 0.08 gm tri sodium citrate (El Gomhoria Co. Egypt, 95%) and 0.2 g Polyvinylpyrrolidone (PVP) (ICN Biomedials, Inc., Av. Wt 30,000–40,000) was dissolve in 10 ml water with stirring. After complete dissolve 75 ml of 0.01 M $AgNO_3$ Silver nitrate (Riedel-de Haën Wt.169.87) was added to the reaction mixture, followed by the rapid addition of the reducing agent (0.1 M $NaBH_4$) Sodium borohydride (Sigma, 98%).. The addition of the reducing agent resulted in the formation of yellow-colored spherical AgNPs, as indicated by previous studies [37–39].

2.2 2-Preparation of CoAgNC

A cheap and straightforward method was used to prepare cobalt nanoparticles (CoNPs), in which metal salt reduction occurred in a controlled environment with an appropriate reducing agent. Firstly, 1 gm PVA Polyvinylalcohol (PVA) (Fluka, Av. Wt. 22,000). was dissolved in 20 ml water, heated to 60°C. After complete disolve, 3 ml (0.05M) Cobalt Cobaltous chloride hexahydrate (WINLAB, 98%).was added, and finally, 5 ml (0.05 M) sodium borohydride was added dropwise with continuous stirring until the solution became completely dark, indicating CoNP formation.

As CoNPs have low stability in air due to their smaller size, they were coated with AgNPs to stabilize them. CoAgNC was prepared chemically by reducing silver nitrate in the presence of pre-synthesized CoNPs, which acted as "seeds" or nucleation sites for the resultant CoAgNC. For the preparation of CoAgNC, 10 ml CoNPs in an aqueous medium were placed in a 100 ml flask equipped with a small magnet bar for stirring. Then, 10 ml (0.05 M) $AgNO_3$ was added dropwise while stirring, and simultaneously, 5 ml (0.05 M) sodium borohydride was slowly injected to avoid mass production of pure AgNPs. During the reduction process, a yellowish color developed, indicating the formation of AgNPs.

2.3 3-Preparation of IOAgNC

To prepare magnetite nanoparticles (IONPs), 2.7 gm $FeCl_3$ Ferric chloride anhydrous (LOBA Chemicals, 98%).was dissolved in 25 ml distilled water, and then 10 ml (0.6 M $NaCo_3$) Sodium carbonate (Riedel-de Haën, Wt.106) was added, and the mixture was stirred for around 10 min. Afterwards, 0.12 gm ascorbic acid (El Nasr Pharmaceutical Chemicals Co. Egypt, Wt. 176) was dissolved in 10 ml distilled water and added rapidly to the reaction mixture, and the entire mixture was stirred for 15 min. The formation of IONPs was confirmed by the appearance of a black color.

To prepare IOAgNC, 10 ml of (6×10^{-3} M) prepared IONPs as a seed solution was taken, then add to 10 ml of 0.001 M $AgNO_3$ with stirring for 15 min then 5 ml of 0.005 M $NaBH_4$ were slowly added with constant stirring to allow the formation of silver magnetite nanocomposite.

2.4 4-Photostability of AgNPs, CoAgNC and IOAgNC

The photostability of the prepared AgNPs, CoAgNC, and IOAgNC was assessed by subjecting them to different light sources, including UV light of 254 nm and light emitting diodes (LEDs) emitting at 490 nm and 250 mW. Before the solutions were exposed to the light sources, the absorption spectra of the solutions were measured. The solutions were then irradiated with the light sources, and the absorption spectra were measured at different time intervals to monitor any changes. The shape and size of the AgNPs in the obtained solution were investigated using a spectrophotometer and TEM after irradiation for several time intervals.

2.5 Characterization of AgNPs, CoAgNC and IOAgNC

A double beam UV–Vis-NIR spectrophotometer (Cary 5000, Agilent, Santa Clara, USA) with a quartz cell in the wavelength range of 200–900 nm was used to characterize the produced nanomaterial. A High-Resolution Transmission Electron Microscope (HRTEM, Tecnai, G20, FEI, Almelo, Netherlands) operated at an Accelerating Voltage of 200 kV was used to image the morphology. A copper grid was coated with carbon, and a few drops of the diluted produced samples were placed on the grid and let the sample to dry at room temperature. Vibrating sample magnetometer (VSM) EV11 (Model 8810), ADE Technologies, Inc. was used to test the magnetic characteristics.

2.6 Biological assessment

2.6.1 Cell culture

HEp-2 cells preserved by cryopreservation at – 85 °C were thawed and passaged in growth medium containing 10% serum. The cells, which included normal control, dark control, light control, and treated cells, were planted at a density of 100 cells per mm^2 on 24-well culture plates for further study.

2.7 Dark toxicity assessment

Four replicates of cells were tested for AgNPs, CoAgNC, and IOAgNC. AgNPs was tested at various concentrations, such as 100 µM, 200 µM, and 300 µM, whereas IOAgNC was tested at greater concentrations, such as 500 µM, 1000 µM, and 1500 µM. The cells were exposed to the produced nanomaterials for five and twenty-four hours, respectively.

2.8 Light toxicity assessment

Cells used for treatment were exposed to blue light LED of 460 nm and 200 mW when treated with AgNPs, CoAgNC, and IOAgNC. The same concentrations of nanomaterials were used for treatment as those in the dark control experiments. Light exposure was performed at 100, 200, 300, and 400 J for cells incubated with Ag, CoAgNC, and IOAgNC. All light experiments were conducted at both 5-h and 24-h time points following incubation with the

nanomaterials. In all experiments, cells were washed twice with PBS at the end of the required incubation time to remove excess NPs. Maintenance medium was added to the cells before exposing them to the appropriate monochromatic light.

2.9 Staining of viable cells

To stain viable cells, a volume of 800 µL of 0.0075% Neutral Red dye (Nice Chemicals, N42109) diluted in maintenance EMEM media was added to each well. Three hours were spent incubating the cells at 37 °C. Neutral Red dye was removed from the cells after staining, and the cells were then rinsed with 0.9% NaCl solution and dried using filter paper.

2.10 Cell lysis and measurement of viability

To induce cell lysis, 200 µl of lysis buffer (1-part absolute ethanol, 1-part distilled water, and 0.02 parts glacial acetic acid) were added to each well. This caused the cell membranes of viable cells to rupture, releasing a red color. The absorbance of the released color was measured at 545 nm using an ELISA machine (Awareness Technology Incorporation, Stat Fax – 2100) at the Cancer Biology unit of the National Cancer Institute.

3 Results and discussion

3.1 Characterization of AgNPs, CoAgNC and IOAgNC

The preparation of AgNPs was carried out as described in the experimental section by reducing silver ions using NaBH4 in the presence of a mixture of PVP and sodium citrate as a capping material. The resulting particles exhibited absorption in the visible range due to Surface Plasmon Resonance at 405 nm, and TEM images revealed that the particles were spherical with a very uniform size distribution of about 10 nm. Figure 1a shows the absorption spectra, which display a narrow band, indicating the spherical shape of the particles, as confirmed by the TEM images in Fig. 2a.

The ability to synthesize CoNPs with narrow size distributions and controlled properties has significant potential for the development of magnetic sensors and medical diagnostic devices. CoNPs are typically synthesized through the reduction of Co salts or thermal decomposition of organometallic precursors; however, electron beam vapor deposition has also been employed to produce metallic CoNPs [40, 41]. For the use of magnetic NPs such as cobalt or iron oxides in aqueous-based ferrofluids, the particles must be dispersible in water. While

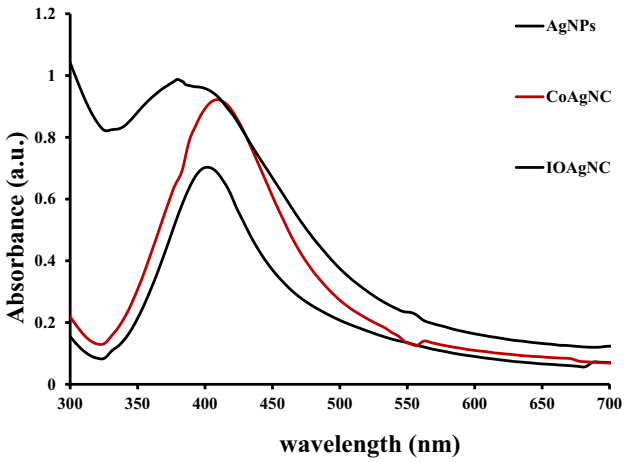

Fig. 1 Absorption spectra of AgNPs, CoAgNC and IOAgNC

most methods reported in the literature utilize an organic phase and organic ligands and surfactants to stabilize the prepared nanomaterials, we aimed to synthesize CoNPs in a water-based solution using PVA as a surfactant. This method enables the preparation of CoNPs in an aqueous phase, making them applicable for biological applications, and it offers the advantages of a simple and inexpensive chemistry.

In this study, CoNPs were synthesized by reducing the metal salt using a strong reducing agent in the presence of a long-chain surfactant at a predetermined concentration to ensure colloidal stability. The polar functional groups of the polymer were utilized to create significant hydrogen bonding between the surface of the CoNPs and the polymer chains, which may also have facilitated cross-linking between the polymer chains.

It is important to note that the synthesis procedure for CoAgNC involves two stages: the first stage involves the reduction of cobalt ions, while the second stage involves the reduction of silver ions in the presence of prepared CoNPs as seeds. The process can be described using the following chemical equations: Firstly, cobalt ions are reduced by NaBH4 according to the equation:

$$4Co^{+2} + NaBH_4 + 3H_2O \rightarrow 4Co^0(metal) + Na^+ + B(OH)_3 + 7H^+.$$

And hydrogen gas is by-produced according to Equation:

$$NaBH_4 + 4\,H_2O \rightarrow NaOH + B(OH)_3 + 4H_2(gas).$$

Subsequently, silver ions are reduced by hydrogen gas produced through the hydrolysis of sodium borohydride. This results in the formation of Ag atoms that diffuse to Co metals, leading to the formation of CoAgNC. These bimetallic nanocomposites are stable in aqueous

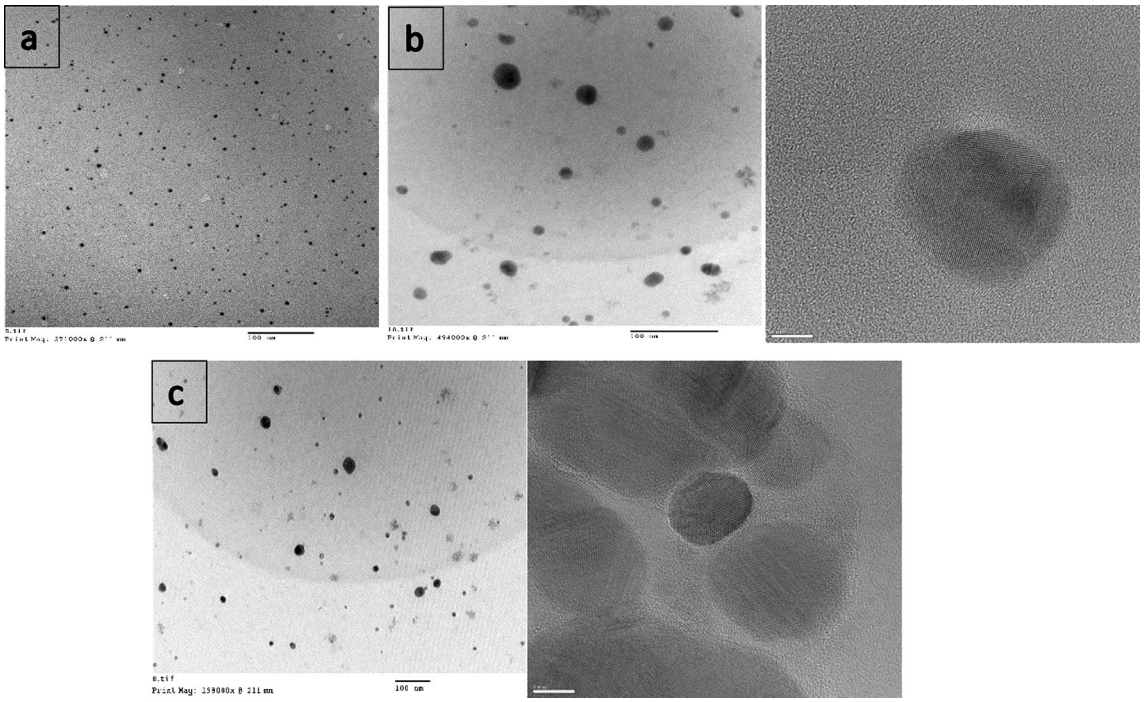

Fig. 2 TEM Images for **a** AgNPs, **b** CoAgNC and **c** IOAgNC (magnification 5 nm, 100 nm)

solution for several months without the observation of cobalt oxide. The optical absorption study provides more evidence for bimetallic nanocomposites. The appearance of the plasmon band for the AgNPs indicates that silver metal coexists with the CoNPs. The UV–Vis absorption spectra for CoAgNC show a sharp absorption peak at 413 nm, as depicted in Fig. 1b. This red shift indicates the formation of bimetallic CoAgNC its size about 20 nm, which is confirmed by the TEM images in Fig. 2b.

Due to their biocompatibility, biodegradability, ease of manufacture, tunability, and functionalization for particular applications, iron oxide nanoparticles (IONPs) containing nanocrystalline magnetite (Fe_3O_4) offer tremendous promise in oncological treatment. Additionally, superparamagnetic behavior is seen in spherical magnetite NPs with diameters less than 20 nm, which is a characteristic that can improve contrast in magnetic resonance imaging (MRI). A biocompatible coating that offers enough functional groups for the conjugation of additional tumor-targeting and therapeutic compounds is often included in superparamagnetic iron oxide nanoparticle (SPION) conjugates in addition to magnetite, which naturally provides MRI contrast [42–45].

The synthesis procedure for IOAgNC involves two stages: the first stage involves the preparation of IONPs, while the second stage involves the reduction of silver ions in the presence of prepared IONPs as seeds. Firstly, water-soluble IONPs were prepared by reacting $FeCl_3$ with sodium carbonate in the presence of ascorbic acid, which acted as both a reducing and capping agent. IONPs could be readily disseminated in hydrated aqueous environments because they were coated with $C_6H_6O_6$, which is ascorbic acid's oxidation state. The following was proposed as a potential formation mechanism for the magnetite nanocrystals:

$$2Fe^{3+} + 3CO_3^{2-} + 6H_2O \rightarrow 2Fe(OH)_3 + 3H_2CO_3$$

$$2Fe(OH)_3 + C_6H_8O_6 \rightarrow 2Fe(OH)_2 + C_6H_6O_6 + 2H_2O$$

$$2Fe(OH)_3 + Fe(OH)_2 \rightarrow Fe_3O_4 + 4H_2O$$

In this system, adding Na_2CO_3 caused the red $FeCl_3$ solution to become yellow, suggesting that $Fe(OH)_3$ had been produced as a result of the hydrolysis of Fe^{3+}. The color of the reaction system changed from yellow to black as soon as ascorbic acid was added to the colloid solution. These IONPs become water-soluble and biocompatible by ascorbic acid capping. These findings are in line with earlier research by Shouhu et al. [46] who found an average size of 5.2 nm for IONPs. These magnetite particles were used as seeds to grow a hybrid nanostructure of silver, combining magnetic properties with plasmonic metallic characteristics. This hybrid was formed by reducing silver ions using hydrogen gas produced from the hydrolysis of sodium borohydride, according to the following equations:

$$NaBH_4 + 4\,H_2O \rightarrow NaOH + B(OH)_3 + 4H_2(gas).$$

Subsequently, the produced Ag atoms diffused onto the surface of IONPs, leading to the formation of IOAgNC. The absorption band of the AgNPs should appear at 400 nm due to the surface Plasmon resonance of spherical AgNPs; however, in this case, it appears at 392 nm, as shown in Fig. 1. This blue shift may be attributed to the change in the dielectric constant of the surrounding environment due to the presence of the Fe_3O_4NPs its size about 15nm, which is confirmed by the TEM images in Fig. 2c.

3.2 Photostability of AgNPs, CoAgNC and IOAgNC

Figure 3a clearly shows that when the prepared AgNPs were irradiated with UV light, the intensity of the plasmon band at 405 nm decreased, and a new feature began to emerge on the red side. Continuous irradiation led to an increase in this new feature until it reached its maximum after 2 h of irradiation. Further irradiation using UV light led to a decrease in both bands, the original plasmonic and the new band that appeared at 550 nm. It was important to identify the origin of this new band, so the same experiment was repeated, and TEM images were taken after 120 min of irradiation. The TEM images in Fig. 3b indicate the formation of some prisms.

The same experiment was repeated using LED to irradiate the sample at 490 nm. Figure 3d shows that some rods and prisms were formed due to irradiation. It is worth noting that irradiation using LED to the formation of a new band at 595 nm, as shown in Fig. 3c, and this band remained stable even after irradiation for seven hours. This implies that irradiation using a Light Emitting Diode caused the transformation of the spherical particles into more anisotropic shapes, while irradiation using UV light resulted in the formation of larger particles that eventually aggregated.

Cobalt has one of the largest magnetic susceptibilities among the common iron oxide and other transition metals. However, it readily oxidizes upon exposure to air, resulting in an antiferromagnetic oxide layer of CoO. Therefore, coating CoNPs with an oxygen-impermeable sheath would provide numerous benefits. In our synthesis of CoAgNC, it was essential to ensure the protection of the Co nanocrystals against oxidation from the surrounding environment as well as from oxidation by light or air. The need for the photostability of Co or CoAgNC is significant because of their use in the treatment of cancer

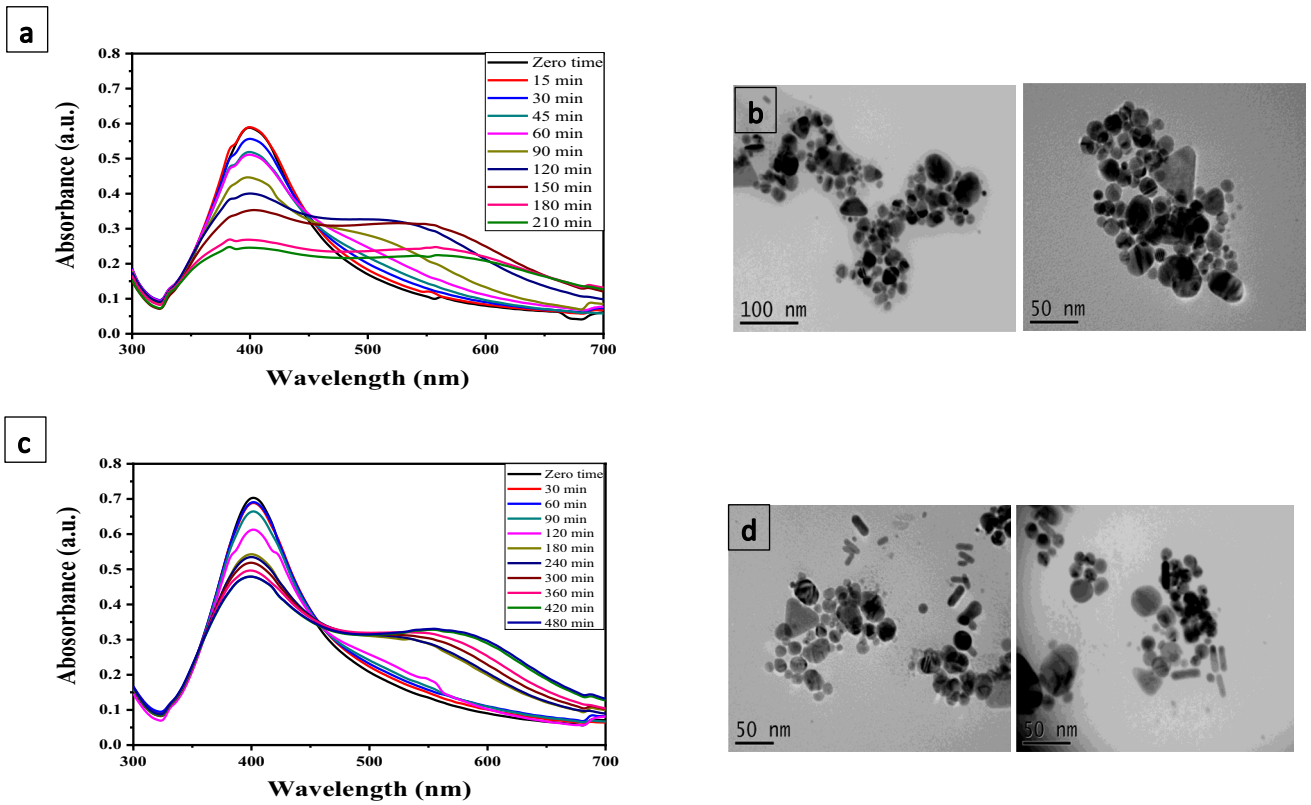

Fig. 3 Effect of irradiation by UV-light on the AgNPs, **a** absorption curves, **b** TEM Images (magnification 50 nm, 100 nm). Effect of irradiation by light emitting diode (LED) on the AgNPs, **c** absorption curves, **d** TEM Images (magnification 50 nm)

as hyperthermic agents in magnetic fluid hyperthermia. When these particles are exposed to light, the target tissue or cells are also exposed. We tested the stability of CoAgNC by exposure to two sources of light, UV, and visible light, as observed in Fig. 4a, c. However, irradiation of CoAgNC using UV light or LED had no effect on the stability of the particles due to the little lattice mismatch between cobalt and silver, as both have a cubic lattice structure. It is apparent from Fig. 4b, d that irradiation of IOAgNC using UV light or LED to the complete decomposition of the particles in the solution. This might be due to the lattice mismatch between magnetite IONPs and AgNPs.

3.3 Magnetic properties of IOAgNC and CoAgNC

To obtain magnetic property measurements on CoAgNC and IOAgNC magnetic property measurements on CoAgNC and IOAgNC, a vibrating sample magnetometer (VSM) was utilized. For each measurement, a hysteresis loop was generated, and from this loop, the intrinsic coercivity (Hc), remanent magnetization (Mr), and saturation magnetization (Ms) were calculated.

The magnetic hysteresis loops for CoAgNC and IOAgNC were measured using a vibrating sample magnetometer (VSM) at room temperature (300 K), as shown in Fig. 5a and b, respectively. CoAgNC exhibited a wider hysteresis loop and higher magnetic moment (MS) of about 1.321549 emu/g, with a switching field (HC) of 5.3172 T (5317.2 Oe) and a remanence MR of 0.84059 emu/g. The remanence ratio MR/MS (Squarence ratio SQR) was about 0.636064. IOAgNC, on the other hand, had a magnetic moment (MS) of about 0.61449 emu/g, with a switching field (HC) of 0.6536 T (653.6 Oe) and a remanence MR of 0.142463 emu/g. The remanence ratio MR/MS (Squarence ratio SQR) was about 0.2318. These results indicate that CoAgNC and IOAgNC possess magnetic properties that make them suitable candidates for cancer therapy and imaging. The AgNPs in these nanocomposites have photothermal properties due to the strong absorption of light resulting from their surface Plasmon, which can efficiently convert into heat. Moreover, magnetic NPs have strong magnetic properties that make them useful for imaging via MRI.

3.4 In vitro assessment of prepared nanomaterials on HEp-2 human laryngeal carcinoma cell

The focus of this study is to establish an in vitro model using the HEp-2 human laryngeal carcinoma cell line to assess the potential efficacy of photothermal agents as a promising approach for cancer therapy. The photothermal nanomaterials under investigation are AgNPs, CoAgNC, and IOAgNC.

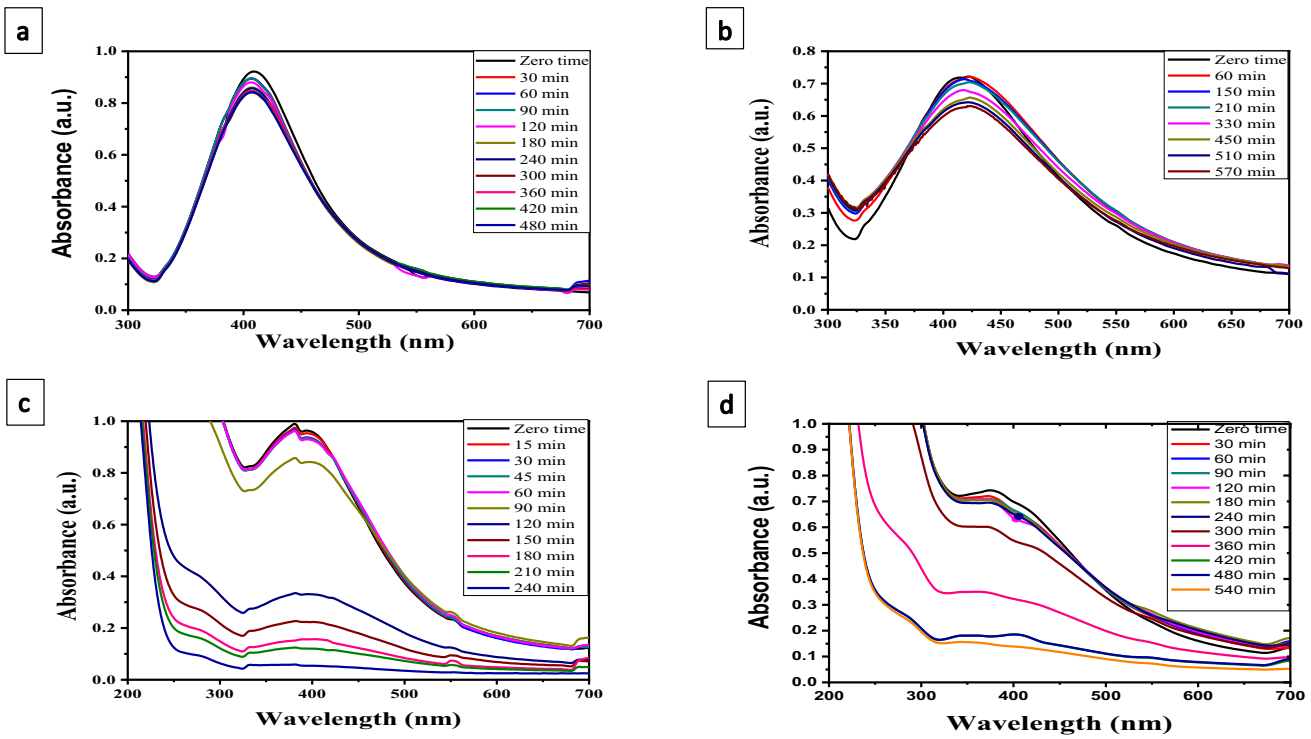

Fig. 4 Effect of irradiation UV-light on **a** CoAgNC, **b** IOAgNC and Effect of irradiation by LED on **c** CoAgNC. **d** IOAgNC

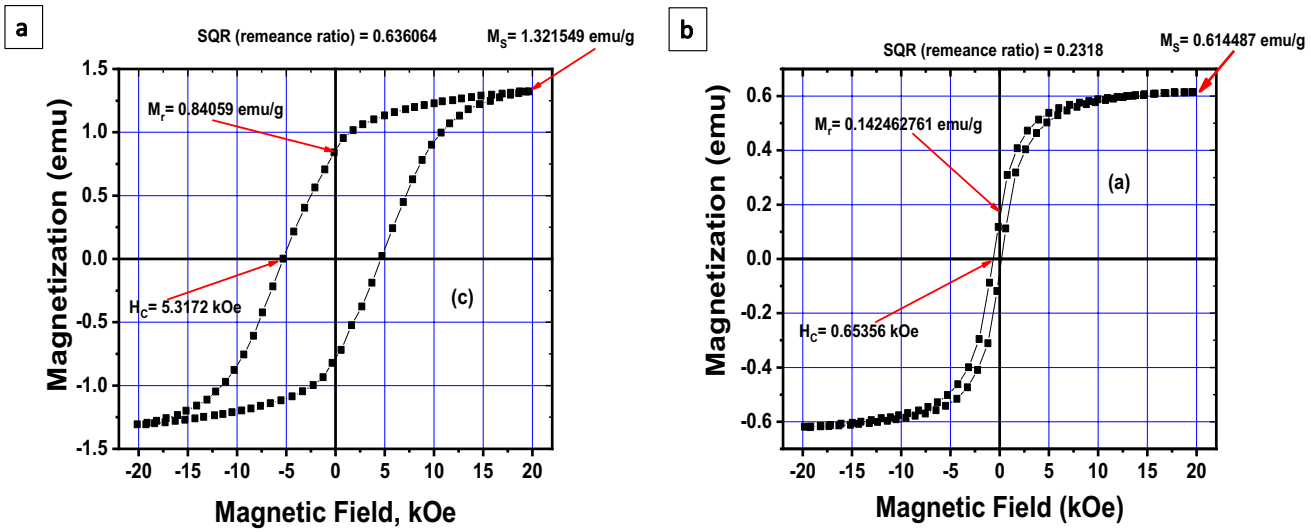

Fig. 5 Hysteresis loop for **a** CoAgNC, **b** IOAgNC

3.5 Dark toxicity of AgNPs, CoAgNC and IOAgNC on HEp-2 cell line

To rule out toxic concentrations in the absence of light exposure and to monitor the selectivity of the applied therapeutic modality, the cellular toxicity of the tested nanomaterials was evaluated. As shown in Fig. 6a, concentrations less than 0.1 mM of AgNPs exhibited negligible toxicity to HEp-2 cells compared to the normal control. As the concentration increased above 0.1 mM, cellular viability slightly decreased, indicated by 66.87, 63.24, and 59.38% at 0.1, 0.2, and 0.3 mM, respectively, after 5 h of incubation. After 24 h of incubation, the viability was 58.1, 54.97, and 68.16% at the same concentrations. The higher

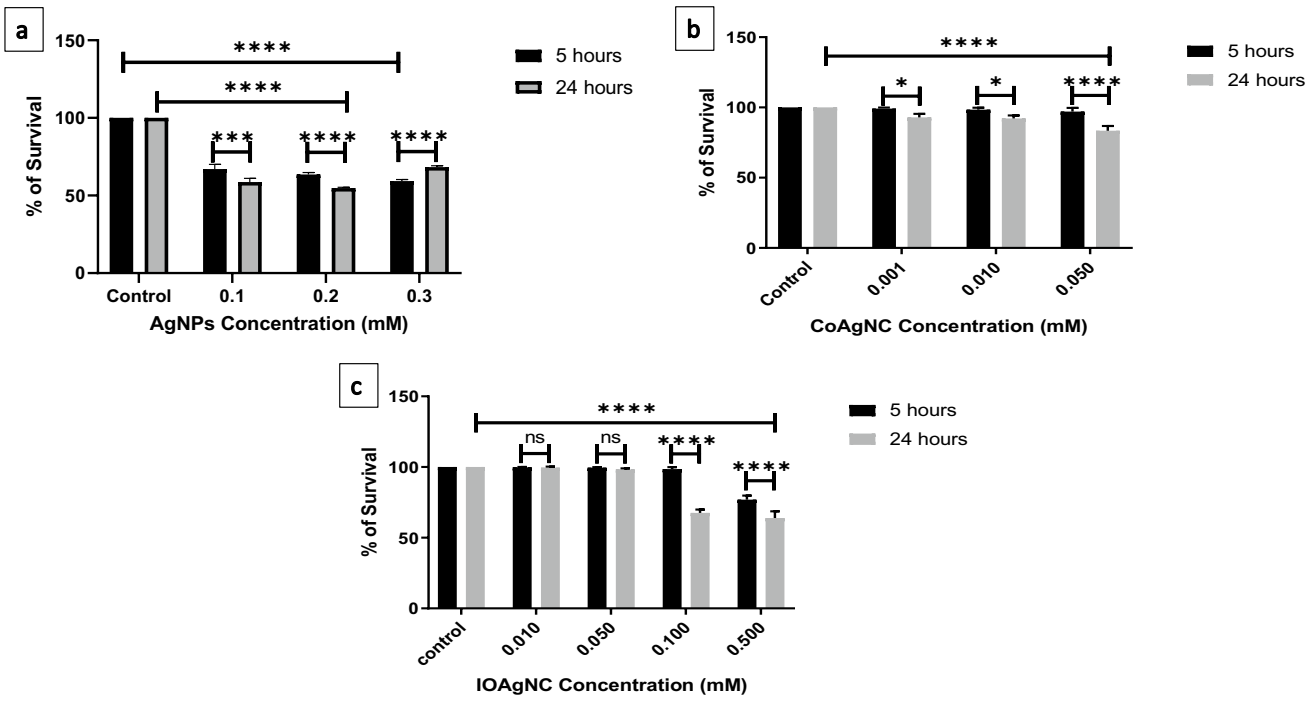

Fig. 6 Dark toxicity test on HEp-2 cells at different concentrations (mM) on % survival of HEP-2 cells after incubation with **a** AgNPs, **b** CoAgNC and **c** IOAgNC for 5 and 24 h

viability of cells observed after 24 h for the 0.3 mM concentration compared to 0.1 and 0.2 mM could be attributed to the increased rate of release of the high nanomaterial dose introduced into each cell, or it might also be due to some experimental technical artifacts.

Figure 6b illustrates the effect of CoAgNC on the viability of HEp-2 cells at different concentrations and incubation periods. As seen in the figure, CoAgNC had no cytotoxic effect on the cells at all concentrations for an incubation period of 5 h. However, as the incubation time increased, the cytotoxic effect of CoAgNC began to increase. As expected, higher concentrations and longer incubation periods resulted in a higher cytotoxic effect of the nanoparticles on cell viability. The percentage of cell survival when incubated with 5×10^{-2} mM for 5 h was 100%, but it decreased to 83.7% when incubated for 24 h. Although there was a decrease in the percentage of cell survival at 24 h, it did not significantly affect the cells' viability.

Figure 6c revealed that concentrations of 0.01, 0.05, and 0.1 mM had no effect on cell viability after a 5-h incubation period, compared to the normal control cells. Meanwhile, they showed comparable results at 24 h, apart from 0.1 mM, where cell viability decreased to 67%. Higher concentrations of IOAgNC had a significant impact on cell viability, exhibited by 74.3% at 0.5 mM after a 5-h incubation period and 60% viability at the same concentrations when cells were incubated with IOAgNC for 24 h.

The higher toxicity observed at 24 h compared to 5 h can be attributed to the increased stress on the cells after prolonged incubation with the nanomaterials. Continuous release and uptake of nanomaterials over 24 h can disrupt the chemical and physiological functions of the cells, potentially interfering with cell organelles or lipids, thereby decreasing cell viability. This feature was less apparent after only 5 h of incubation.

3.6 Light control and photothermal therapy of HEp-2 laryngeal carcinoma cells using AgNPs, CoAgNC and IOAgNC

A control experiment was performed to assess the light source's effect on HEp-2 cell line viability without the prepared nanomaterials. This was done to confirm that the previous results were obtained solely due to the activation of the nanomaterials by the light emitting diode, as shown in Fig. 7a.

In Fig. 7a, it can be observed that the average survival rate decreases as the exposure light dose increases. This slight decrease in the survival percentage indicates that the light source has a cytotoxic effect on the HEp-2 cell line. However, the cytotoxic effect of light is not significant,

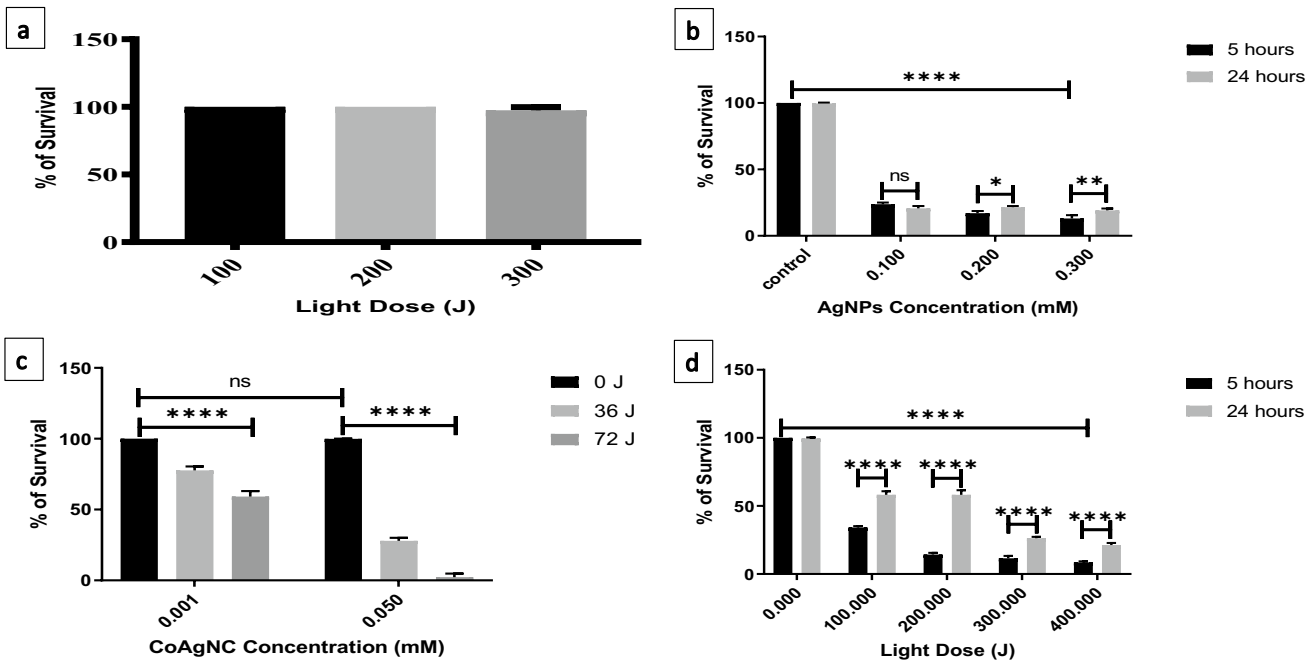

Fig. 7 **a** The effect of 120 mW, 490-nm light LED on % survival of HEP-2 cell line in the absence of nanomaterials. **b** Effect of a laser light dose (200 J) on different AgNPs concentrations. **c** % survival of HEP-2 cells at different exposure times when exposed to 120 mW, 490 nm blue LED incubated with 10^{-6} and 5×10^{-5} M/L CoAgNC. **d** Effect of different light doses on tumor cells viability incubated with 0.5 mM of IOAgNC at different time points

and there is no noticeable effect of light on cell mortality in the results obtained.

In Fig. 7b HEp-2 cells were exposed to various concentrations of AgNPs and 200 J of monochromatic LED with blue light of 460 nm and 200 mW. Significant decreases in cellular viability were observed at different time points. When a certain dose of light was applied to different concentrations of AgNPs, it was observed that after 5 h, viability decreased to half by increasing the concentration from 0.1 to 0.2 mM, but then only decreased slightly by increasing the concentration to 0.3 mM. However, after 24 h, there was no noticeable decrease in cell viability by increasing the nanomaterial concentration. This suggests that 5 h is a more suitable time point than 24 h, attributed to the release of AgNPs from the cells at longer incubation times. Therefore, this graph demonstrates that the light dose can be the limiting factor determining the extent of cell viability more than the nanomaterial concentration.

Starting with the least concentration of 10^{-3} mM of CoAgNC, in Fig. 7c we exposed the cells to different light doses, and as expected, a higher light dose resulted in a lower percentage of cell survival. Figure 7c compares the effects of different concentrations of nanomaterials on HEp-2 cell viability. As shown in the figure, after 36 J of light exposure, the percentage of cell survival at 5×10^{-2} mM was less than half the percentage survival for 10^{-3} mM. Therefore, the cytotoxic effect of 5×10^{-2} mM of CoAgNC is twice the effect caused by 10–3 mM after the same light dose. After 72 J of light exposure, the percentage of cell survival was 0% for 5×10^{-2} mM, meaning that all cells died. From this, we can conclude that the cytotoxic effect of CoAgNC depends on the concentration of the nanomaterial used.

In Fig. 7d, HEp-2 tumor cells incubated with 0.5 mM of IOAgNC were exposed to different doses of blue light of 460 nm and 200 mW at 100, 200, 300, and 400 J. Measurements of cell viability showed a clear decrease, indicated by 34, 12.86, 11.2, and 9% at 100, 200, 300, and 400 J, respectively, after 5 h of incubation with IOAgNC. However, when cells were incubated for 24 h with the same concentration of nanomaterials and exposed to the same light doses, viability was found to be 58.6, 58.3, 25.5, and 21%, respectively. The results showed a gradual decrease in cell viability by increasing the dose of light exposure. It was also evident that treating the cells with light after 5 h of incubation with nanomaterials induced higher toxicity to the cells than after 24 h. This can be attributed to the relative ratio between the rates of uptake versus release of IONPs after 24 h. If the rate of uptake were slower than the rate of release, this could explain the lower toxicity observed after 24 h, but this was not the case. At 5 h of incubation time, the cells had taken up IONPs at a higher rate than releasing them, since they had been recently introduced to the cells. The results also showed that increasing the light dose from 100 to 200 J resulted in a significant increase in cell cytotoxicity, while no significant difference was found by increasing the light dose to 300 or 400 J.

4 Conclusion

The integration of nanomaterials and biology leading to major advances in the life sciences. Recent advances have involved the development of functional optical, or magnetic nanoparticles conjugated to biomolecules. A special class of nanomaterials is the nanocomposite system of high magnetic moment, such as IOAgNC and CoAgNC, which can be synthesized using simple and inexpensive chemistry. These nanomaterials have significant potential for tumor treatment through magnetic fluid hyperthermia, and thus, their photostability, chemical stability, and biocompatibility were investigated. We reported the synthesis of Ag, CoAgNC, and IOAgNC in an aqueous solvent and characterized using UV–vis spectrophotometer, TEM, VSM.The potential toxicity of the prepared nanomaterials was performed using the Hep-2 cell line and indicated that these systems show no toxicity even at high concentrations of the nanocomposite. Also we investigated the photothermal effects of the nanocomposites by irradiating the cells of interest with UV and LED at different concentrations and light doses. The cells exposed to light irradiation suffered damage and thermal explosion, demonstrating that plasmon resonant silver nanocomposites are highly effective at transforming light into heat and Thus, AgNPs, CoAgNC, and IOAgNC are good potential candidates.

Acknowledgements We would like to acknowledge primarily Dr. Al-Sayed El-Sherbini and Dr. Mona Bakr for their efforts, guidance and supporting with everything we need both personally and scientifically in this research and we hope that God had mercy on them.

Authors' contributions MAR and TAET designed and performed all experiments, analyzed the data, and approved the final manuscript.

Funding Open access funding provided by The Science, Technology & Innovation Funding Authority (STDF) in cooperation with The Egyptian Knowledge Bank (EKB). This research did not receive any specific grant from funding agencies in the public, commercial, or not-for-profit sectors.

Data availability The datasets used and/or analyzed during the current study are available from the corresponding author on reasonable request.

Declarations

Competing interests All the authors declare they have no competing interests.

Ethical approval Approval reverence: NILES – EC - CU 23/7/11.

Consent to participate Not applicable.

Consent for publication Current study is available from the corresponding author on reasonable request.

References

1. Mikhaylova M, Kim DK, Bobrysheva N et al (2004) Superparamagnetism of magnetite nanoparticles: dependence on surface modification. Langmuir 20(6):2472–2477
2. Chen M, Yamamuro S, Farrell D et al (2003) Gold-coated iron nanoparticles for biomedical applications. J Appl Phys 93(10):7551–7553
3. Faid AH, Shouman SA, Badr YA et al (2022) Enhanced cytotoxic effect of doxorubicin conjugated gold nanoparticles on breast cancer model. BMC Chem 16(1):90
4. Mohamad EA, Ramadan MA, Mostafa MM et al (2023) Enhancing the antibacterial effect of iron oxide and silver nanoparticles by extremely low frequency electric fields (ELF-EF) against S aureus. Electromagn Biol Med. https://doi.org/10.1080/15368378.2023.2208610
5. Mostafa MM, Mohamad EA, Ramadan MA et al (2022) Reduced graphene Oxide @ Magnetite nanocomposite and ELFEF effect on Staphylococcus aureus growth inhibition. Egypt J Chem 66(6):267–278
6. Arun T, Verma SK, Panda PK et al (2019) Facile synthesized novel hybrid graphene oxide/cobalt ferrite magnetic nanoparticles based surface coating material inhibit bacterial secretion pathway for antibacterial effect. Mater Sci Eng C 104:109932
7. Verma SK, Panda PK, Kumari P et al (2021) Determining factors for the nano-biocompatibility of cobalt oxide nanoparticles: proximal discrepancy in intrinsic atomic interactions at differential vicinage. Green Chem 23(9):3439–3458
8. Makkar H, Verma SK, Panda PK et al (2018) In vivo molecular toxicity profile of dental bioceramics in embryonic zebrafish (Danio rerio). Chem Res Toxicol 31(9):914–923
9. Verma SK, Jha E, Panda PK et al (2019) Biological effects of green-synthesized metal nanoparticles: a mechanistic view of antibacterial activity and cytotoxicity. In: Naushad M, Rajendran S, Gracia F (eds) Advanced nanostructured materials for environmental remediation. Springer, Cham, pp 145–171
10. Roath S (1993) Biological and biomedical aspects of magnetic fluid technology. J Magn Magn Mater 122(1–3):329–334
11. Papisov MI, Bogdanov A Jr, Schaffer B et al (1993) Colloidal magnetic resonance contrast agents: effect of particle surface on biodistribution. J Magn Magn Mater 122(1–3):383–386
12. Widder K, Flouret G, Senyei A (1979) Magnetic microspheres: synthesis of a novel parenteral drug carrier. J Pharm Sci 68(1):79–82
13. Catherine CB, Adam SGC (2003) Functionalisation of magnetic nanoparticles for applications in biomedicine. J Phys D Appl Phys 36(13):R198
14. Stoeva SI, Huo F, Lee J-S et al (2005) Three-layer composite magnetic nanoparticle probes for DNA. J Am Chem Soc 127(44):15362–15363
15. Safari J, Farkhondeh Masouleh S, Zarnegar Z et al (2014) Water-dispersible Fe_3O_4 nanoparticles stabilized with a biodegradable amphiphilic copolymer. C R Chim 17(2):151–155
16. Faid AH, Shouman SA, Badr YA et al (2022) Gold nanoparticles loaded chitosan encapsulate 6-mercaptopurine as a novel nanocomposite for chemo-photothermal therapy on breast cancer. BMC Chem 16(1):94–94
17. Wang L, Luo J, Fan Q et al (2005) Monodispersed core-shell Fe_3O_4@Au nanoparticles. J Phys Chem B 109(46):21593–21601
18. Sharifi M, Hasan A, Nanakali NMQ et al (2020) Combined chemo-magnetic field-photothermal breast cancer therapy based on porous magnetite nanospheres. Sci Rep 10(1):5925
19. Bossmann SH, Payne MM, Kalita M et al (2022) Iron-based magnetic nanosystems for diagnostic imaging and drug delivery: towards transformative biomedical applications. Pharmaceutics 14(10):2093
20. Zhang D, Du Y (2006) The biocompatibility study of Fe_3O_4 magnetic nanoparticles used in tumor hyperthermia. In: 2006 1st IEEE international conference on nano/micro engineered and molecular systems
21. Zeng H, Li J, Wang ZL et al (2004) Bimagnetic core/shell FePt/Fe_3O_4 nanoparticles. Nano Lett 4(1):187–190
22. Ramadan MA, Sharaky M, Faid AH (2022) Ionic gelation synthesis, characterization and cytotoxic evaluation of chitosan nanoparticles on different types of human cancer cell models. Egypt J Chem 65(2):153–159
23. Salazar-Alvarez G, Sort J, Suriñach S et al (2007) Synthesis and size-dependent exchange bias in inverted core–shell MnO|Mn_3O_4 nanoparticles. J Am Chem Soc 129(29):9102–9108
24. El-Sayed MA (2001) Some interesting properties of metals confined in time and nanometer space of different shapes. Acc Chem Res 34(4):257–264
25. Nour M, Hamdy O, Faid AH et al (2022) Utilization of gold nanoparticles for the detection of squamous cell carcinoma of the tongue based on laser-induced fluorescence and diffuse reflectance characteristics: an in vitro study. Lasers Med Sci 37(9):3551–3560
26. LaVan DA, Lynn DM, Langer R (2002) Moving smaller in drug discovery and delivery. Nat Rev Drug Discov 1(1):77–84
27. Macchi S, Jalihal A, Hooshmand N et al (2022) Enhanced photothermal heating and combination therapy of NIR dye via conversion to self-assembled ionic nanomaterials. J Mater Chem B 10(5):806–816
28. Davies R, Schurr GA, Meenan P et al (1998) Engineered particle surfaces. Adv Mater 10(15):1264–1270
29. Templeton AC, Wuelfing WP, Murray RW (1999) Monolayer-protected cluster molecules. Acc Chem Res 33(1):27–36
30. Faid AH, Shouman SA, Thabet NA et al (2022) Laser enhanced combinatorial chemo-photothermal therapy of green synthesis gold nanoparticles loaded with 6mercaptopurine on breast cancer model. J Pharm Innov 18:144–148

31. Kalele S, Gosavi SW, Urban J et al (2006) Nanoshell particles: synthesis, properties and applications. Current Sci 91(8):1038–1052
32. Ocana M, Hsu WP, Matijevic E (1991) Preparation and properties of uniform-coated colloidal particles. 6. Titania on zinc oxide. Langmuir 7(12):2911–2916
33. Makarova OV, Ostafin AE, Miyoshi H et al (1999) Adsorption and encapsulation of fluorescent probes in nanoparticles. J Phys Chem B 103(43):9080–9084
34. Ethiraj AS, Hebalkar N, Kulkarni SK et al (2003) Enhancement of photoluminescence in manganese-doped ZnS nanoparticles due to a silica shell. J Chem Phys 118(19):8945–8953
35. Kalele SA, Kundu AA, Gosavi SW et al (2006) Rapid detection of Escherichia coli by using antibody-conjugated silver nanoshells. Small 2(3):335–338
36. Smith JN, Meadows J, Williams PA (1996) Adsorption of polyvinylpyrrolidone onto polystyrene latices and the effect on colloid stability. Langmuir 12(16):3773–3778
37. Ali MM, Ramadan MA, Ghazawy NA et al (2022) Photochemical effect of silver nanoparticles on flesh fly larval biological system. Acta Histochem 124(1):10
38. Amin RM, Mohamed MB, Ramadan MA et al (2009) Rapid and sensitive microplate assay for screening the effect of silver and gold nanoparticles on bacteria. Nanomedicine 4(6):637–643
39. Métraux GS, Mirkin CA (2005) Rapid thermal synthesis of silver nanoprisms with chemically tailorable thickness. Adv Mater 17(4):412–415
40. Dinega DP, Bawendi MG (1999) A solution-phase chemical approach to a new crystal structure of cobalt. Angew Chem Int Ed 38(12):1788–1791
41. Puntes VF, Krishnan KM, Alivisatos AP (2001) Colloidal nanocrystal shape and size control: the case of cobalt. Science 291(5511):2115–2117
42. Polo E, Collado M, Pelaz B et al (2017) Advances toward more efficient targeted delivery of nanoparticles in vivo: understanding interactions between nanoparticles and cells. ACS Nano 11(3):2397–2402. https://doi.org/10.1021/acsnano.7b01197
43. Weissleder R, Stark DD, Engelstad BL et al (1989) Superparamagnetic iron oxide: pharmacokinetics and toxicity. AJR Am J Roentgenol 152(1):167–173
44. Stephen ZR, Kievit FM, Zhang M (2011) Magnetite nanoparticles for medical MR imaging. Mater Today 14(7–8):330–338
45. Revia RA, Zhang M (2016) Magnetite nanoparticles for cancer diagnosis, treatment, and treatment monitoring: recent advances. Mater Today 19(3):157–168
46. Xuan S, Hao L, Jiang W et al (2007) Preparation of water-soluble magnetite nanocrystals through hydrothermal approach. J Magn Magn Mater 308(2):210–213